Journal of Molecular Graphics and Modelling 29 (2011) 818–825

Contents lists available at ScienceDirect

Journal of Molecular Graphics and Modelling

journal homepage: www.elsevier.com/locate/JMGM

Insight into analysis of interactions of GW9508 to wild-type and H86F and H137F GPR40: A combined QM/MM study and pharmacophore modeling

Shao-Yong Lu[a], Yong-Jun Jiang[b,*], Jian-Wei Zou[b], Hai-Bin Luo[c], Tian-Xing Wu[a]

[a] Department of Chemistry, Zhejiang University, Hangzhou, Zhejiang 310027, PR China
[b] Key Laboratory for Molecular Design and Nutrition Engineering, Ningbo Institute of Technology, Zhejiang University, No. 1 Qianhunana Road, Ningbo, Zhejiang 315104, PR China
[c] School of Pharmaceutical Sciences, Sun Yat-Sen University, Guangzhou 510006, PR China

ARTICLE INFO

Article history:
Received 19 November 2010
Received in revised form 13 January 2011
Accepted 13 January 2011
Available online 1 February 2011

Keywords:
GPR40
ONIOM
NH–π interaction
Pharmacophore model
Molecular docking
Type 2 diabetes

ABSTRACT

GPR40 is a novel potential target for the treatment of type 2 diabetes. In this work, a two-layered ONIOM based QM/MM approach was employed to study the interactions between GW9508 and GPR40: wild-type, H86F, and H137F mutated systems. The calculated results clearly indicated that His137 is directly involved in ligand recognition through the NH–π interaction with the GW9508. In contrast, His86 is not interacting with the GW9508 in the NH–π interaction. The interaction energies, calculated at the MP2/6–31(d, p) level, were performed to gain more insight into the energetic differences of the wild-type and two mutated systems at the atomistic level. In addition, the obtained pharmacophore model was well consistent with structure–functional requirements for the binding of GPR40 agonists and with per-residue energy decomposition of the ONIOM calculations.

1. Introduction

GPR40, which has been named free fatty acid receptor 1, predominantly expressed in pancreatic β-cell and activated by physiological concentrations of free fatty acids (FFAs) [1–3], is a member of the G-protein coupled receptor (GPCR) superfamily. It is well-established that GPR40 is mainly coupled with $G\alpha_q/G\alpha_{11}$, which activates phospholipase C, resulting in the formation of inositol 1,4,5-triphosphate and induction of calcium release from endoplasmic reticulum [4–6]. Indeed, FFAs increase intracellular calcium concentrations and lead to amplify glucose-stimulated insulin secretion from pancreatic β-cell via GPR40. Therefore, the implication of GPR40 in insulin secretion has attracted considerable attention to the receptor as a novel potential therapeutic target for the treatment of type 2 diabetes.

Drug discovery endeavors have already discovered many GPR40 synthetic ligands [7–11] and some of these compounds are at various stages of development. Recently, a novel series of agonists originated from 3-(4-{*N*-alkylamino}phenyl) propanoic acid was described by GlaxoSmithKline, where compound GW9508 appears to be the preferred one (EC_{50} = 64.6 nM) [8,9]. Sum et al. [12] investigated the molecular determinants contributing to binding of linoleic acid and GW9508. Their results confirmed that GW9508 and linoleic acid are anchored on their carboxylate groups by Arg183, Asn244, and Arg258. Moreover, His86, Tyr91, and His137 contribute to aromatic and/or hydrophobic interactions with GW9508. Furthermore, Tikhonova et al. [13] proposed a polarized NH–π interaction between His137 and GW9508 as one of the contributing forces leading to the high potency of GW9508 based on the H137F mutant.

Intermolecular force of the NH–π contact has been the subject of intense interest from both experimental and theoretical points of view due to their fundamental role in crystal packing, protein–ligand recognition, and drug design. The crystal structure of ammonia channels in a membrane sheds light on the important interactions regarding the NH–π contact in the transport of ammonia [14]. In the protein kinase Chk1, addition of a substituted phenyl ring, methoxyphenol ring, to a weak Chk1 kinase inhibitor increased affinity from 8.5 to 0.026 μM [15]. This is partially ascribed to the additional phenyl ring forms, an NH–π contact with the polar amide N–H of Ser147. The NH–π interactions in His–aromatic complexes are stabilized by π–π, δ^+–π (NH–π) and/or cation–π interactions according to whether the His is in the neutral or protonated state [16]. The frequent occurrences of His–aromatic interactions at protein–DNA

* Corresponding author. Tel.: +86 574 88229517; fax: +86 574 88229516.
E-mail addresses: yjjiang@nit.zju.edu.cn, yjjiang@nit.net.cn (Y.-J. Jiang).

1093-3263/$ – see front matter © 2011 Elsevier Inc. All rights reserved.
doi:10.1016/j.jmgm.2011.01.006

interfaces [17], in ion channels [18], in GPCRs [19], and in enzymes [20] emphasize their importance in biological processes.

Molecular mechanics and empirical force field, attributed to a number of factors including inaccurate or incomplete force field parameters, do not yield this NH–π weak interaction. For large molecules of biological relevance, however, it is not feasible to apply full quantum chemical treatment. The large size of biological systems prohibits the efficient use of electronic structure methods with a reasonable computational cost. Recently, one powerful hybrid method known as the combined quantum mechanics/molecular mechanics (QM/MM) method, e.g., our own N-layered integrated molecular orbital and molecular mechanics (ONIOM) method developed by Morokuma and co-workers [21,22] has been successfully applied to the study of several biomacromolecular systems [23–25]. The advantage of using ONIOM method is that the most critical part of the system can be treated with high level of QM methods, while the remaining part can be calculated using MM methods. Based on the ONIOM methodology, the system of interest, which is defined as the bound complex of GW9508 in its binding pocket consisting of amino acids His86 and His137 or mutated amino acids, can be employed with the accurate QM method, and the residues surrounding this inner model can be treated with a lower level of theory calculations.

The ligand-based 3D pharmacophore can help medicinal chemists visualize the potential interaction between ligand and receptor, as well as can be used as a query in 3D database search to identify new structural classes of potential lead compounds [26,27]. Thus, the construction of an accurate pharmacophore is a critical objective in rational drug design. Currently, Kurogi and Guner [28] have employed Catalyst/HipHop generated pharmacophore method to identify novel mesangial cell proliferation inhibitors. Michaux et al. [29] identified 16 diverse and highly cyclooxygenase-2 (COX-2) selective inhibitors by generating pharmacophore model via Catalyst/HipHop approach. These researches indicate that Catalyst/HipHop generated pharmacophore can be effectively used for identifying new potential lead candidates.

In the present work, first, a two-layer ONIOM-based QM/MM method was established for study of the GPR40–GW9508 interaction concerning the H86F and H137F mutations. The following work describes how the binding interactions of GW9508 to the wild-type and mutants of the GPR40–GW9508 complex. Detailed knowledge of the interaction between GW9508 and the binding site of GPR40 can provide a structural explanation for the structure-based drug design of GPR40 agonists. Second, in an attempt to gain further insight into the structural requirements for GPR40 agonists, a Catalyst/HipHop pharmacophore model was developed. This pharmacophore model highlights the important binding features of GPR40 agonists, and may provide guidance for the rational design for discovering novel GPR40 agonists.

2. Materials and computational methods

2.1. System setup

The coordinates of the validated GPR40–GW9508 complex are available in the literature [13]. The binding site for GW9508 was experimentally verified by Tikhonova and co-workers via site-mutagenesis [12,13]. The construction of H86F and H137F mutants was carried out with the Protein Modeling module of Discovery Studio 2.1 (DS 2.1) [30], using the wild-type GPR40–GW9508 complex as a template and replacing target residues with the desired amino acid. Residues centered on the mutated residues within 4.5 Å were optimized and finally five minimized models were created, respectively. The structure with the lowest energy scores (DOPE score in DS 2.1) in the respective five models was chosen as the candidate for the following ONIOM calculations.

2.2. ONIOM hybrid calculations

The main objective of the ONIOM study is to understand the NH–π weak interactions between His86, His137, and π-systems of GW9508 in GPR40. To achieve this, QM/MM calculations were performed with the use of two-layer ONIOM scheme: the ligand GW9508, the residues His86 and His137, and Phe86 or Phe137 in the corresponding mutated systems were in the QM layer, while the remaining residues were in the MM layer. Hydrogen atoms were used as capping atoms. For the QM layer, Becke's three parameter hybrid functional with the correlation functional of Lee, Yang, and Parr (B3LYP) [23–25] and the basis set 6–31G(d) were used. The MM layer of the systems was treated by means of the AMBER parm96 force field. The restricted electrostatic-potential (RESP) fitting procedure was employed to obtain partial atomic charges of GW9508, and the generalized amber force field (GAFF) package [31] was used for parameters not found in the AMBER force field. In this study, electrostatic interactions between the two layers, where do not involve in the chemical reactions, were calculated using mechanical embedding (ME) scheme. In the ME scheme, they were calculated at the MM level. In contrast, in the electronic embedding (EE) scheme, the electrostatic interactions between the two layers are treated by including certain one-electron terms in the QM Hamiltonian. The polarization of the QM layer by the charge distribution of the MM layer is also taken into account automatically, leading to the increased computational cost. However, the QM/MM-EE scheme has been applied to study on the related GPCR-rhodopsin regarding to calculate the total energy of the system [32–35].

2.3. Interaction energy calculations

The experimentally supported binding pocket in the transmembrane containing 16 residues is depicted in Fig. 1. The interaction energies ($\Delta E_{(\mathrm{GW9508}+X_i)}$) between the ligand GW9508 and individual residues (X_i), which were calculated as a single point energy calculation at the Møller–Plesset second-order perturbation theory (MP2) in conjugation with the basis set 6–31(d, p), including basis set superposition error (BSSE) corrections [36], were assessed from Eq. (1).

$$\Delta E_{(\mathrm{GW9508}+X_i)} = E_{(\mathrm{GW9508}+X_i)} - E_{(\mathrm{GW9508})} - E_{(X_i)} + \mathrm{BSSE} \quad (1)$$

where $\Delta E_{(\mathrm{GW9508}+X_i)}$ is the interaction energy, $E_{(\mathrm{GW9508}+X_i)}$ is the energy of the complex, $E_{(\mathrm{GW9508})}$ and $E_{(X_i)}$ are the energies of ligand GW9508 and individual residue, respectively. All of these calculations were carried out with the help of Gaussian 03 suite of programs [37].

2.4. Generation of pharmacophore hypotheses with HipHop

Pharmacophore hypotheses generation was performed by Catalyst/HipHop implemented in DS 2.1. Catalyst/HipHop generates pharmacophore hypothesis using active compounds only. Thus, four P-amino/hydroxyl-substituted phenyl propionic acid derivatives, shown in Fig. 2, were selected as a training set to develop the pharmacophore model. Conformational models for the molecules were developed by poling algorithm, which seeks to provide a broad coverage of conformational space using the best conformer generation method with a maximum conformational energy of 20 kcal/mol [38]. The number of conformers generated for each compound was limited to a maximum of 250. The agonists were classified based on activity using the principal property in the DS 2.1. A value of 2 was aligned to the compound 1 as a reference

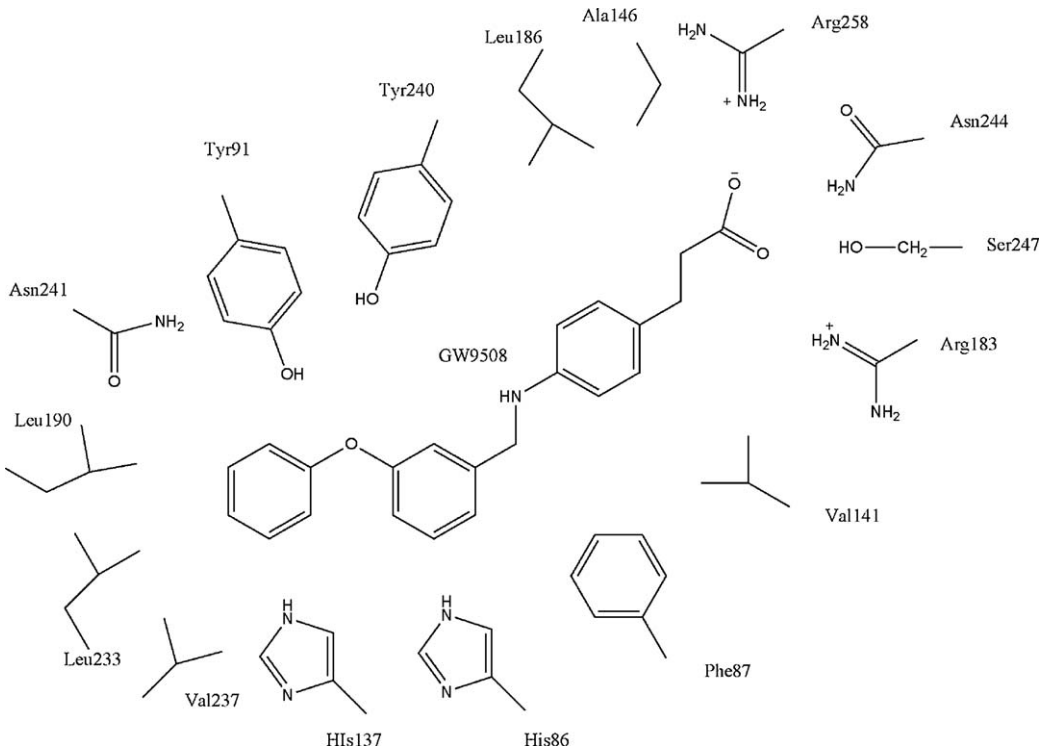

Fig. 1. Schematic representation of the model system consisting of 16 residues in the transmembrane.

with the most activity and a value of 1 for the rest compounds. Given the chemical nature of the four compounds studied in this work, the following six chemical functions were selected in the feature dictionary: hydrogen bond acceptor, hydrogen bond donor, hydrophobic, hydrophobic aromatic groups, negative ionizable, and ring aromatic. All other settings were kept as a default. Pharmacophores were then computed using the Common Feature Pharmacophore Generation module of DS 2.1 and the top 10 scoring hypothesis were exported. The best one was selected for further studies.

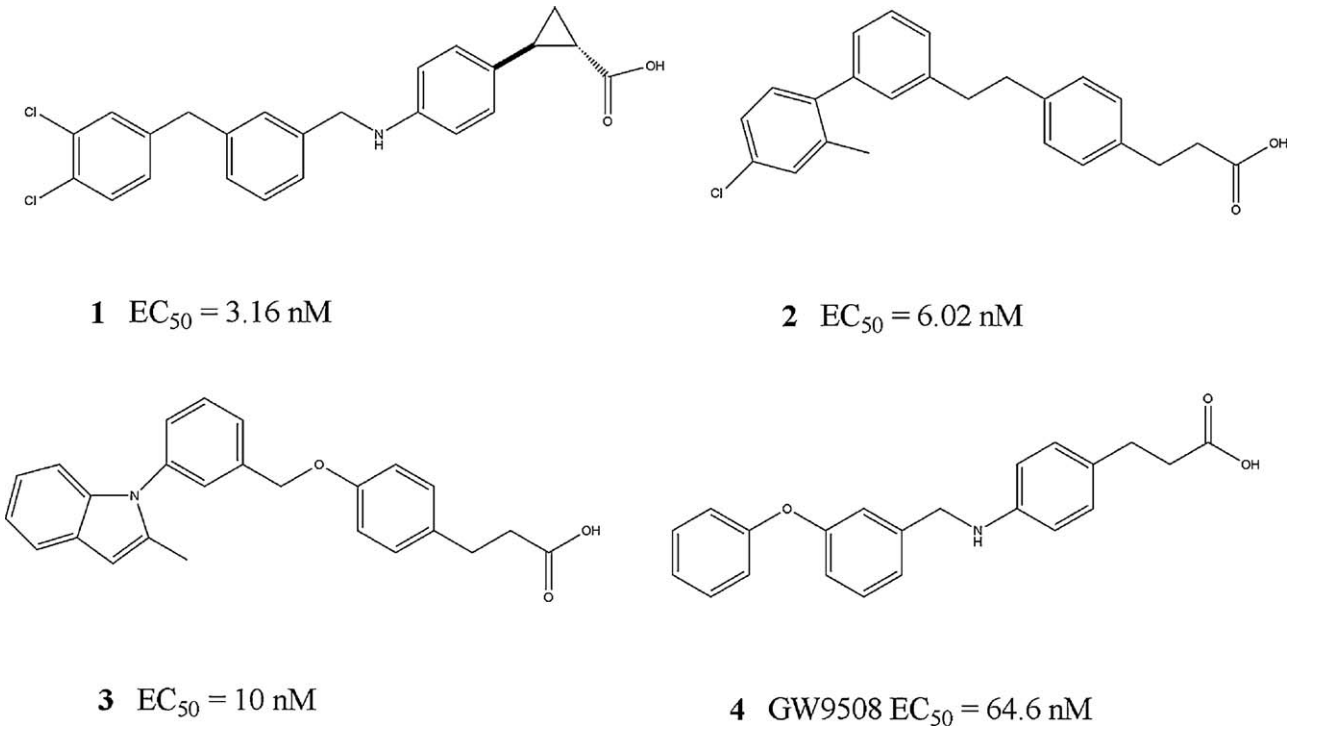

Fig. 2. Four molecular structures of GW9508 analogs forming the training set used to obtain HipHop pharmacophore hypothesis. (1) Ref. [40], (2) Ref. [41], (3) Ref. [42], and (4) Ref. [9].

2.5. Molecular docking study

Docking of the compound 1 into the binding site of GPR40 was performed using the AutoDock4.2 software package [39]. Polar hydrogen atoms were added by using the Hydrogen module in AutoDock Tools (ADT) for GPR40. After that, Kollman united atom partial charges were assigned for the receptor and the AutoDock atom types were defined using ADT, graphical user interface of AutoDock provided by MGL Tools. For the compound 1, all hydrogen atoms were added and the default root, rotatable bonds, and torsion of the inhibitors were set through TORSDOF module in ADT. The grid maps of 60, 60, and 60 points in *x*, *y*, and *z* direction were built centered on the center of the corresponding inhibitors with the help of AutoGrid, with a spacing of 0.375 Å between the grid points. The distance-dependent function of the dielectric constant was employed to calculate the energetic maps.

The Lamarckian genetic algorithm (LGA) was used for the ligand conformational search with the following settings: a maximum number of 25,000,000 energy evaluations, an initial population of 150 randomly placed individuals, a maximum number of 27,000 generations, a mutation rate of 0.02, a crossover rate of 0.80, and an elitism value of 1. Finally, 50 independent docking runs were carried out for the compound 1.

3. Results and discussion

3.1. NH–π interaction of His–aromatic in GPR40

The imidazole cycle of histidine has a pK_a value of 6.1 and can exist in two kinds of states, neutral or protonated, under physiological conditions. When histidine is neutral, it can contact with its aromatic partner in π–π interactions or δ^+–π (NH–π) interactions, due to polarizable interactions. When histidine is protonated, it can form cation–π interactions with its aromatic partner, due to electrostatic contributions [16]. In the present study, we focus on the His residue in its neutral form to interact with the aromatic partner of GW9508, in order to analyze the effect of NH–π interaction on the binding affinity.

In the literature, different sets of parameters are used to describe the NH–π geometry; here, we use the set given in Fig. 3. Parameters α, β, *D*, and *d* have the following meaning: α and β are the molecular planes of both interacting partners, *D* is the distance from the nitrogen atom of the imidazole cycle to the centroid of the aromatic ring (N···Cg), and *d* defines the distance from the hydrogen atom to the centroid of the aromatic ring (H···Cg). The NH–π interactions were identified according to a distance and an angle criteria [43]. The distance requires an intermolecular distance varying from 2.8 to 4.0 Å for *D*, and from 1.8 to 3.0 Å for *d*, respectively. The His–aromatic pairs were divided into T-shape and stacked conformations, according to whether the dihedral between the two planes is higher or lower than 45°.

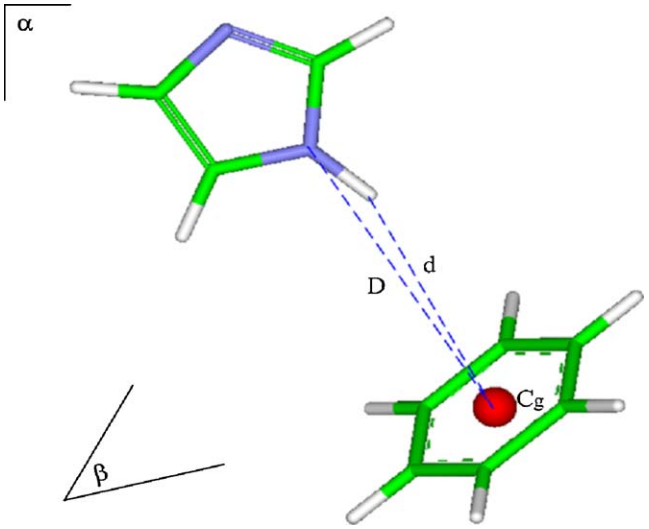

Fig. 3. Geometrical parameters used for the analysis. Imidazole and benzene are employed here as a model histidine, π-system, respectively. Carbon, nitrogen, hydrogen atoms are drawn in green, blue and white, respectively. Phenyl ring centroid is in red as sphere. The molecular planes of the imidazole and of the aromatic species are α and β, respectively. *D* is the distance between the nitrogen atom and the centroid of the aromatic ring, while *d* is the distance between the hydrogen atom and phenyl ring centroid. (For interpretation of the references to color in this figure legend, the reader is referred to the web version of the article.)

The optimized structures of the QM layer of the full models for GPR40–GW9508 complex for the three systems at the level of ONIOM (B3LYP:AMBER) are shown in Fig. 4. The calculated distances and dihedrals between the histidine and the corresponding aromatic ring according to each studied model are summarized in Table 1 by comparison between the wild-type and two mutants. From the Table 1, it is clear that the calculated distances *D* and *d* are 3.88 and 3.00 Å between the His137 and the terminal phenoxy ring of GW9508 in the wild-type, respectively, which forms a typical NH–π interaction according to the distance criterion of this weak interaction. Moreover, the dihedral of the molecular planes of both interacting partners is lower than 45°, as in the case of the stacked conformation. However, the His86 did not involve in the NH–π interaction with the benzylamino ring of GW9508 in the wild-type system, due to the calculated distances beyond this criterion, with the values of 5.60 and 5.62 Å, respectively. Inspection of Table 1, for the H86F mutant, reveals that the distances *D* and *d* for the His137–aromatic interaction are slightly larger than the conventional NH–π interaction, with the values of 4.30 and 3.40 Å,

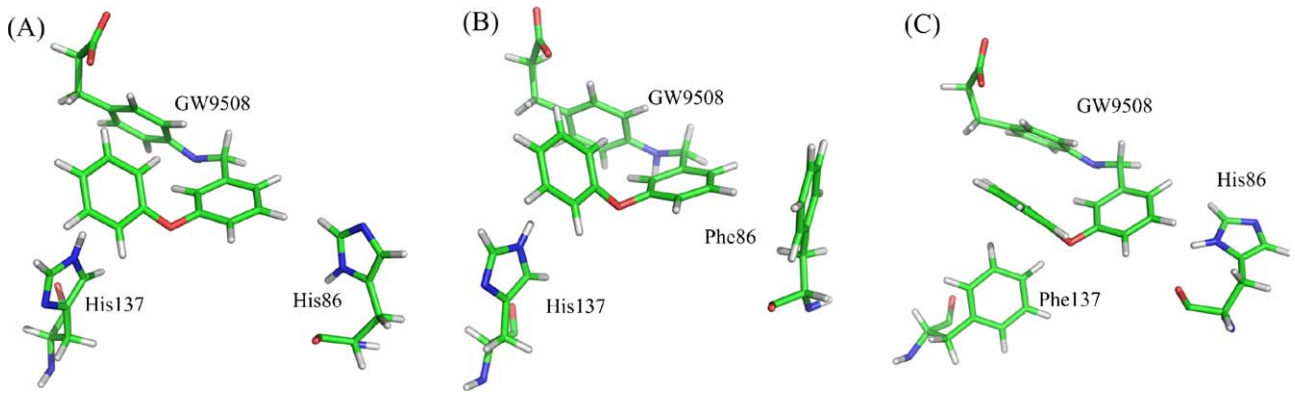

Fig. 4. Optimized structures of the QM layer of the full models at the ONIOM (B3LYP:AMBER) level. (A) Wild-type system, (B) H86F mutant, and (C) H137F mutant.

Table 1
Distance values for N···Cg (D) and H···Cg (d), and dihedral angle (θ) for plane α and β after ONIOM calculations for the three systems.

	D (N···Cg) (Å)			d (H···Cg) (Å)			θ (°)		
	WT	H86F	H137F	WT	H86F	H137F	WT	H86F	H137F
H86[a]	5.60	–	4.3	5.62	–	3.5	70	–	20
H137[b]	3.88	4.07	–	3.00	3.40	–	40	25	–

[a] His86 is interacting with the benzylamino ring of GW9508.
[b] His137 is interacting with the terminal phenoxy ring of GW9508.

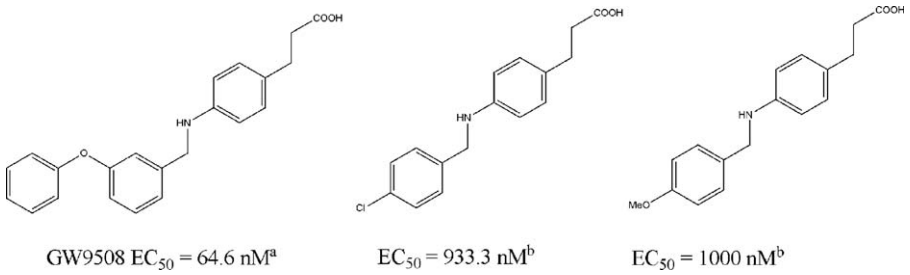

Fig. 5. Activity for the GW9508 and aryl propionic acid. (a) Ref. [9] and (b) Ref. [8].

respectively. For the H137F mutant, the NH–π interaction was no longer present between Phe137 and GW9508. This is consistent with the experimental evidence currently available in the literature that mutation of His86 to Phe had a small effect on the response to agonist GW9508, whereas the H137F mutant had a disruptive effect on the binding of GW9508, diminishing potency by ∼28-fold [12,13]. Therefore, the ONIOM calculations, together with the experimental results, suggest that GW9508 is more likely to interact with His137 than with His86. The remarkable increase in the activity of GW9508 versus aryl propionic acid (Fig. 5) is attributed to the critical role of the NH–π interaction between the His137 and the terminal aromatic ring of GW9508.

3.2. Interaction strength of GW9508 with individual residues (X_i) in the binding pocket

Gaining insight into the individual residue decomposition of total energy will give us a better understanding and more detailed information in the interaction between GW9508 and the binding pocket of GPR40. The residue-based decomposition of interaction energies in the wild-type and two mutants allows us to identify many of the basic features of the interaction with GW9508 and to compare in terms of receptor–ligand interactions between the wide-type and mutated systems.

The interaction energies between GW9508 and each residue that surrounds the binding pocket, collected in Table 2 for the wild-type and two mutants, were calculated on the optimized structures obtained from the two-layer ONIOM calculations. The MP2/6–31G(d, p) method was employed in the single-point energy calculation to take the dispersion interaction into account whereas the density functional theory cannot handle this dispersion interaction, due to the NH–π interaction between receptor and ligand [44,45].

Table 2 lists the energy contributions of the binding pocket residues of interest for the three systems. It is clearly seen that Arg183, Asn244 and Arg258 are predominant energy contributions to GW9508 binding in the wild-type and two mutated systems. In addition, Tyr91, His137, Leu186, and Tyr240, predicted from the individual residue binding energies calculations, appear to be important in the recognition of the GW9508. This is consistent with our previous molecular docking and molecular dynamics studies of GPR40 receptor–agonists interactions [46].

In the H86F mutant, the total individual residue interaction energy was decreased by 2.82 kcal/mol, whereas in the H137F

Table 2
Interaction of GW9508 with individual residues (X_i), calculated by MP2/6–31G(d, p) methods (in kcal/mol).

X_i	Wild-type	H86F mutant	ΔE[a]	H137F mutant	ΔE[b]
His86 (Phe)	−1.00	−2.11	−1.11	−2.83	−1.83
Phe87	−0.36	−1.75	−1.39	−2.81	−2.45
Tyr91	−7.46	−8.33	−0.87	−4.17	**3.29**
His137 (Phe)	−5.70	−5.38	0.32	−0.84	**4.86**
Val141	−2.37	−2.50	−0.13	−1.14	1.19
Ala146	−1.15	−0.48	0.67	−0.40	0.75
Arg183	−63.76	−57.49	6.27	−62.75	1.01
Leu186	−3.85	−3.30	0.55	−3.14	0.71
Leu190	−1.93	−2.16	−0.23	−1.88	0.05
Leu233	0.51	0.42	−0.09	0.38	−0.13
Val237	1.17	1.39	0.22	0.85	−0.32
Tyr240	−3.46	−2.93	0.53	−2.34	1.12
Asn241	0.49	0.08	−0.41	3.21	2.72
Asn244	−20.40	−18.11	2.29	−19.99	0.41
Ser247	−18.21	−18.90	−0.69	−18.69	−0.48
Arg258	−104.89	−108.00	−3.11	−106.00	−1.11
ΔE[c]	0		2.82		9.79

[a] $\Delta E = E_{\text{wild-type}} - E_{\text{H86 mutant}}$.
[b] $\Delta E = E_{\text{wild-type}} - E_{\text{H137 mutant}}$.
[c] The value relative to wild-type.

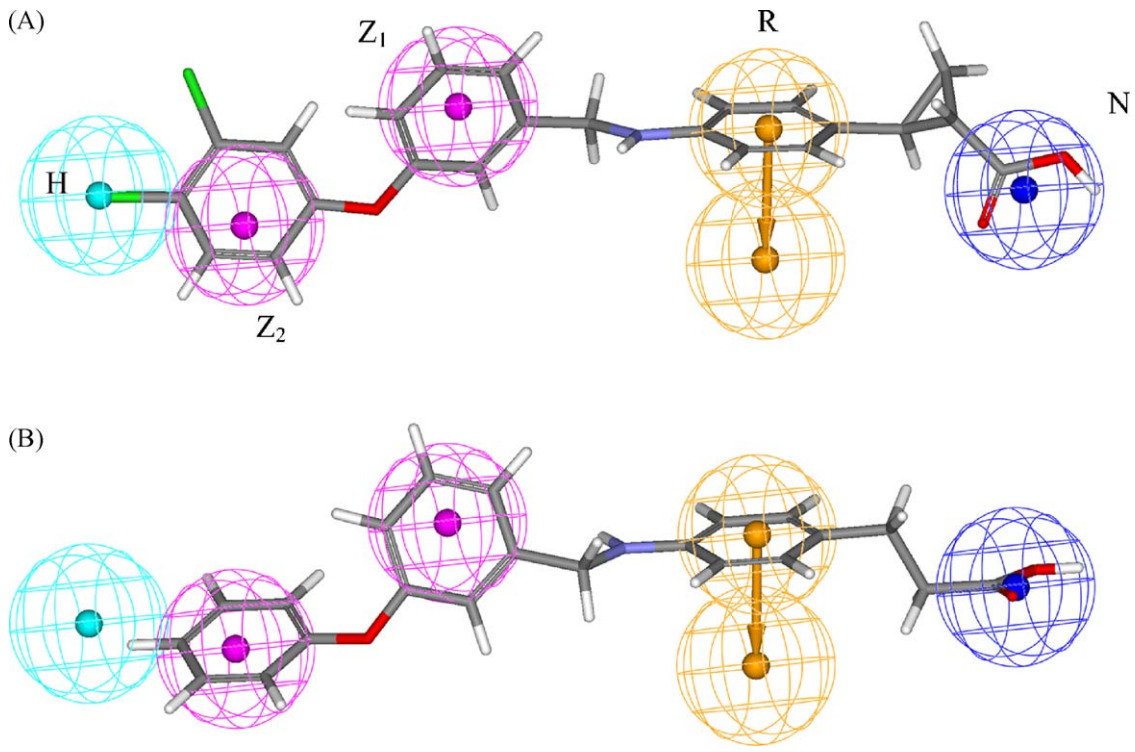

Fig. 6. Training set compound 1 (A) and compound 4 GW9508 (B) mapped to Hypo 1. Hypothesis features are color-coded as follows: negative ionizable (N), blue; ring aromatic (R), yellow; hydrophobic aromatic (Z), magenta; hydrophobic (H), cyan. (For interpretation of the references to color in this figure legend, the reader is referred to the web version of the article.)

mutant, this total interaction energy was significantly reduced by 9.79 kcal/mol (ΔE^c in Table 2), compared to the wild-type system. There are some significant residues that produce the large differences (>3 kcal/mol) between the wild-type and H137F mutant, as highlighted in bold in Table 2. These residues are Tyr91 and Phe137. In the H137F mutant, because the NH–π interaction between Phe137 and terminal phenoxy ring of GW9508 is no longer present, the GW9508 exhibited larger shift in binding pocket relative to the wild-type and H86F mutant. This suggests that the mutated residue (H137F) not only causes the direct effect to the GW9508 but also leads other residues to lose contact or interaction with the GW9508 as well. The obtained binding modes and the calculated interaction energies are in good agreement with the site-directed mutagenesis data. The conservative substitution to Phe caused to a small reduction in potency in H86F albeit led to a greater change in H137F (5.8-fold versus 28-fold) [13].

Table 3
Results of pharmacophore hypothesis generated by HipHop method.

Hypotheses[a]	Features[b]	Rank[c]
Hypo 1	NRZZH	61.84
Hypo 2	NRRZH	61.79
Hypo 3	NRRZH	61.79
Hypo 4	NZZZH	61.72
Hypo 5	NRZZH	61.69
Hypo 6	NRZZH	61.06
Hypo 7	NRRZH	61.02
Hypo 8	NRZZH	60.99
Hypo 9	NRRZH	60.98
Hypo 10	NRRZH	60.98

[a] Numbers for the hypothesis are obtained by the hypothesis generation.
[b] Abbreviations used for features: N, negative ionizable; R, ring aromatic; Z, hydrophobic aromatic; H, hydrophobic.
[c] The ranking score for each hypothesis. Best hypothesis has highest score.

3.3. Pharmacophore model generation

From the results of individual residue interaction energy contributions, a clear notion about the critical residues responsible for the interaction between GW9508 and GPR40 was identified. This knowledge can be used to evaluate the generating 3D-pharmacophore models. The compound 1 was considered as a reference compound, which was allowed to map all features. In contrast, the remaining compounds were allowed to map partially on the features. Finally, 10 five feature hypotheses were generated. The ranking scores of hypothesis range from 60.98 to 61.84, as tabulated in Table 3. The first hypothesis (Hypo 1) was selected for further study due to its best score. The distance and angle parameters between the features of the Hypo 1 are complied in Table 4. From Table 4, it is evident that the distance between the negative ionizable (NI) and ring aromatic (RA) is 5.66 Å, suggesting that a two-carbon tether connecting the carboxylated head group and phenyl ring appears optimal for the aforementioned compounds. Structure–activity relationships revealed that the significantly reduced potency was observed where the two methylenes are replaced with fewer and more methylene groups [9]. This two-carbon tether connecting group provides the proper length required to position the aromatic ring for interaction with Tyr91 and especially with His137.

Fig. 6A and B shows the mapping of Hypo 1 onto the compound 1 and GW9508, respectively. Both features mapped well with reasonable fit values 5.0, and 3.94, respectively. The com-

Table 4
Distances and angles of the GPR40 agonist pharmacophore from this work.

Pharmacophore	Distance range (Å) and angle (°) between features[a]
Hypo 1	N–R 5.66; R–Z_2 6.67; N–Z_1 12.23; N–R–Z_1 164 Z_1–Z_2 5.35; R–Z_2 11.42; R–Z_1–Z_2 144 Z_2–H 3.20; Z_1–H 8.06; Z_1–Z_2–H 140

[a] Abbreviations used for features have the same meaning as in Table 3.

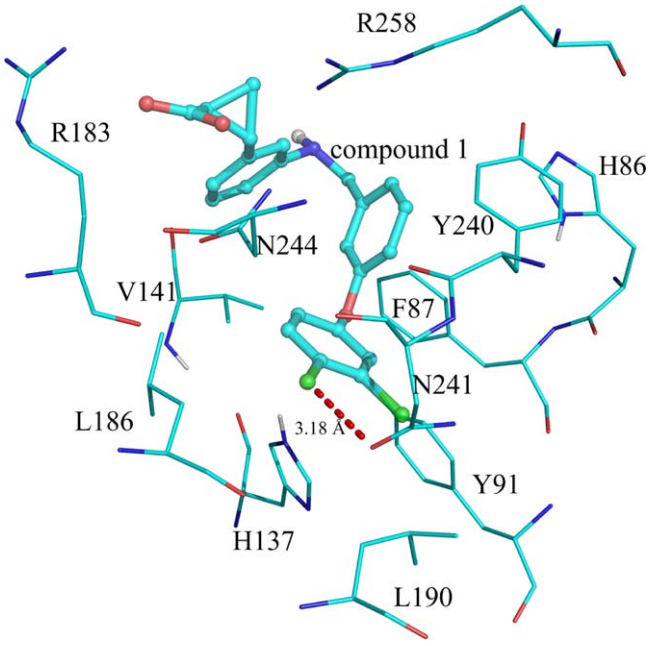

Fig. 7. Binding modes of the compound 1 in the active site of GPR40. The compound 1 is shown in stick and residues in line. The halogen bond is shown in red dotted line.

pound 1 taken as a reference mapped well with five features. On the contrary, the GW9508 mapped with four features except the hydrophobic feature because of no group substitutions in the terminal phenyl ring of GW9508. To validate the possible binding model derived from pharmacophore model Hypo 1, AutoDock was performed to gain insight into the binding mode between the compound 1 and the active site of GPR40. Fig. 7 shows the main interactions between the compound 1 and GPR40. The negative ionizable feature (N) mapped on the carboxylated head group of the compound 1 represents the key hydrogen bonding and electrostatic interactions with Arg183, Asn244, and Arg258 of GPR40. The two hydrophobic aromatic features (Z_1 and Z_2) mapped on the benzylamino ring and terminal phenoxy ring of the compound 1 represent π–π interactions with His86 and Phe87, and NH–π/π–π interactions with Tyr91, His137, and Tyr240, respectively. The hydrophobic feature (H) mapped on the para-substituted chlorine atom locates at the hydrophobic region which is surrounded by Leu186 and Asn241. Moreover, a halogen bond is formed between the chlorine atom and the oxygen atom (OD1) of Asn241, with the distance (Cl···O) and angle (C–Cl···O) of 3.18 Å and 131.6°, respectively. Overall, these observations demonstrate that the proposed pharmacophore model can fit the binding pocket of GPR40 and matches well with the topology of the active site. In addition, these binding modes are coincided with recently published reviews on small-molecular modulators of GPR40. The para-substituted phenyl propionic acid scaffold has emerged as a common structural motif found in many GPR40 agonists, and compounds having an aromatic ring and a group capable of releasing a cation have exhibited excellent agonistic activity [47]. Also, this pharmacophore model is in accordance with the critical residues identified for binding via ONIOM calculations. Based on these results, the obtained pharmacophore could provide a rational hypothetical picture of the primary chemical features responsible for the activity, and is expected to provide useful knowledge in the utility of this pharmacophore model as a 3D query for virtual screening to retrieve novel chemical entities.

4. Conclusions

Two-layer ONIOM calculations were used to investigate the binding modes of GW9508 to the GPR40 binding pocket of the wild-type, H86F, and H137F mutated systems. The calculated results clearly revealed that the His137 is interacting with the terminal phenoxy ring of GW9508 in the NH–π interaction, whereas the His86 is not involved in the NH–π interaction with the benzylamino ring of GW9508 by the geometry analyses of the QM layer derived from the ONIOM calculations. Compared to the wild-type GPR40–GW9508 complex, the H137F mutation eliminates favorable contacts with the Tyr91 and His137, leading to reduce the stability of GW9508 binding. The individual residue energy contributions illustrate that the total energy in the H137F mutant was decreased by 9.79 kcal/mol compared to the wild-type system. This is because of the disruption of the NH–π interaction between the His137 and GW9508. In contrast, in the H86F mutant, the total energy was reduced by 2.82 kcal/mol compared to the wild-type system.

Pharmacophore model based on four GW9508 analogs identified five pharmacophore features, including a negative ionizable, an aromatic ring, two hydrophobic aromatics, and a hydrophobic feature. The pharmacophore model showed that the primary chemical features may be responsible for the activity of the agonists. The type and spatial position of the features are coincided with the pattern of receptor–agonist interactions identified from the ONIOM calculations and from the experimental results. Therefore, the pharmacophore model fulfills the requirements for an effective interaction of agonists with the active site of GPR40 and could be useful for the virtual screening and *de novo* drug design.

Acknowledgments

This work was supported by National High Technology Research and Development Program of China (863 Programs, 2007AA02Z301), Natural Science Foundation of China (No. 20803063) and Natural Science Foundation of Ningbo (No. 2010A610024).

References

[1] N.J. Smith, L.A. Stoddart, N.N. Devine, L. Jenkins, G. Milligan, The action and mode of binding of thiazolidinedione ligands at free fatty acid receptor 1, J. Biol. Chem. 284 (2009) 17527–17539.
[2] C.P. Briscoe, M. Tadayyon, J.L. Andrews, W.G. Benson, J.K. Chambers, M.M. Eilert, C. Ellis, N.A. Elshourbagy, A.S. Goetz, D.T. Minnick, P.R. Murdock, H.R. Sauls Jr., U. Shabon, L.D. Spinage, J.C. Strum, P.G. Szekeres, K.B. Tan, J.M. Way, D.M. Ignar, S. Wilson, A.I. Muir, The orphan G protein-coupled receptor GPR40 is activated by medium and long chain fatty acids, J. Biol. Chem. 278 (2003) 11303–11311.
[3] Y. Itoh, Y. Kawamata, M. Harada, M. Kobayashi, R. Fujii, S. Fukusumi, K. Ogi, M. Hosoya, Y. Tanaka, H. Uejima, H. Tanaka, M. Maruyama, R. Satoh, S. Okubo, H. Kizawa, H. Komatsu, F. Matsumura, Y. Noguchi, T. Shinohara, S. Hinuma, Y. Fujisawa, M. Fujino, Free fatty acids regulate insulin secretion from pancreatic beta cells through GPR40, Nature 422 (2003) 173–176.
[4] A.J. Brown, S. Jupe, C.P. Briscoe, A family of fatty acid binding receptors, DNA Cell Biol. 24 (2005) 54–61.
[5] D.D. Feng, Z. Luo, S.-G. Roh, M. Hernandez, N. Tawadros, D.J. Keating, C. Chen, Reduction in voltage-gated K^+ current in primary cultured rat pancreatic beta-cells by linoleic acids, Endocrinology 147 (2006) 674–682.
[6] H. Shapiro, S. Shachar, I. Sekler, M. Hershfinkel, M.D. Walker, Role of GPR40 in fatty acid action on the beta cell line INS-1E, Biochem. Biophys. Res. Commun. 335 (2005) 97–104.
[7] C. Zhou, C. Tang, E. Chang, M. Ge, S. Lin, E. Cline, C.P. Tan, Y. Feng, Y.-P. Zhou, G.J. Eiermann, A. Petrov, G. Salituro, P. Meinke, R. Mosley, T.E. Akiyama, M. Einstein, S. Kumar, J. Berger, A.D. Howard, N. Thornberry, S.G. Mills, L. Yang, Discovery of 5-aryloxy-2,4-thiazolidinediones as potent GPR40 agonists, Bioorg. Med. Chem. Lett. 20 (2010) 1298–1301.
[8] D.M. Garrido, D.F. Corbett, K.A. Dwornik, A.S. Goetz, T.R. Littleton, S.C. McKeown, W.Y. Mills, T.L. Smalley, T.L. Smalley Jr., C.P. Briscoe, A.J. Peat, Synthesis and activity of small molecule GPR40 agonists, Bioorg. Med. Chem. Lett. 16 (2006) 1840–1845.

[9] S.C. McKeown, D.F. Corbett, A.S. Goetz, T.R. Littleton, E. Bigham, C.P. Briscoe, A.J. Peat, S.P. Watson, D.M.B. Hickey, Solid phase synthesis and SAR of small molecule agonists for the GPR40 receptor, Bioorg. Med. Chem. Lett. 17 (2007) 1584–1589.
[10] S.B. Bharate, A. Rodge, R.K. Joshi, J. Kaur, S. Srinivasan, S.S. Kumar, A. Kulkarni-Almeida, S. Balachandran, A. Balakrishnan, R.A. Vishwakarma, Discovery of diacylphloroglucinols as a new class of GPR40 (FFAR1) agonists, Bioorg. Med. Chem. Lett. 18 (2008) 6357–6361.
[11] E. Christiansen, C. Urban, N. Merten, K. Liebscher, K.K. Karlsen, A. Hamacher, A.D. Spinrath, A.D. Bond, C. Drewke, S. Ullrich, M.U. Kassack, E. Kostenis, T. Ulven, Discovery of potent and selective agonists for the free fatty acids receptor 1 (FFA/GPR40), a potential target for the treatment of type II diabetes, J. Med. Chem. 51 (2008) 7061–7064.
[12] C.S. Sum, I.G. Tikhonova, S. Neumann, S. Engel, B.M. Raaka, S. Costanzi, M.C. Gershengorn, Identification of residues important for agonist recognition and activation in GPR40, J. Biol. Chem. 282 (2007) 29248–29255.
[13] I.G. Tikhonova, C.S. Sum, S. Neumann, C.J. Thomas, B.M. Raaka, S. Costanzi, M.C. Gershengorn, Bidirectional, iterative approach to the structural delineation of the functional "chemoprint" in GPR40 for agonist recognition, J. Med. Chem. 50 (2007) 2981–2989.
[14] S. Khademi, J. O'Connell, J. Remis, Y. Robles-Colmenares, L.J.W. Miercke, R.M. Stroud, Mechanism of ammonia transport by Amt/MEP/Rh: structure of AmtB at 1.35 angstrom, Science 305 (2004) 1587–1594.
[15] N. Foloppe, L.M. Fisher, G. Francis, R. Howes, P. Kierstan, A. Potter, Identification of a buried pocket for potent and selective inhibition of Chk1: prediction and verification, Bioorg. Med. Chem. 14 (2006) 1792–1804.
[16] E. Cauët, M. Rooman, R. Wintjens, J. Liévin, C. Biot, Histidine–aromatic interactions in proteins and protein–ligand complexes: quantum chemical study of X-ray and model structures, J. Chem. Theory Comput. 1 (2005) 472–483.
[17] M. Rooman, J. Liévin, E. Buisine, R. Wintjens, Cation–pi/H-bond stair motifs at protein–DNA interfaces, J. Mol. Biol. 319 (2002) 67–76.
[18] A.M. Lambeir, M. Lauwereys, P. Stanssens, N.T. Mrabet, J. Snauwaert, H. van Tilbeurgh, G. Matthyssens, I. Lasters, M. De Maeyer, S.J. Wodak, J. Jenkins, M. Chiadmi, J. Janin, Protein engineering of xylose (glucose) isomerase from *Actinoplanes missouriensis*. Site-directed mutagenesis of the xylose binding site, Biochemistry 31 (1992) 5459–5466.
[19] Y. Mo, G. Subramanian, J. Cao, D.M. Ferguson, Cation–pi interactions: an energy decomposition analysis and its implication in delta-opioid receptor–ligand binding, J. Am. Chem. Soc. 124 (2002) 4832–4837.
[20] M.A. Argiriadi, C. Morisseau, B.D. Hammock, D.W. Christianson, Detoxification of environment mutagens and carcinogens: structure, mechanism, and evolution of liver epoxide hydrolase, Proc. Natl. Acad. Sci. U.S.A. 96 (1999) 10637–10642.
[21] S. Dapprich, I. Komáromi, S. Byun, K. Morokuma, M.J. Frisch, A new ONIOM implementation in Gaussian98. Part I. The calculations of energies, gradients, vibrational frequencies and electric field derivatives, J. Mol. Struct.: THEOCHEM 461 (1999) 1–21.
[22] T. Vreven, K. Morokuma, O. Frakas, H.B. Schlegel, M.J. Frisch, Geometry optimization with QM/MM, ONIOM, and other combined methods. I. Microiterations and constraints, J. Comput. Chem. 24 (2003) 760–769.
[23] S.-Y. Lu, Y.-J. Jiang, P. Zhou, J.-W. Zou, T.-X. Wu, Geometric characteristics and energy landscapes of halogen–water–hydrogen bridges at protein–ligand interfaces, Chem. Phys. Lett. 485 (2010) 348–353.
[24] J. Ruo, L.-J. Yang, S.-Y. Yang, Binding energy contributions of the conserved bridging water molecules in CDK2-inhibitor complexes: a combined QM/MM study, Chem. Phys. Lett. 460 (2008) 300–305.
[25] S. Saen-oon, O. Aruksakunwong, K. Wittayanarakul, P. Sompornpisut, S. Hannongbua, Insight into analysis of interaction of saquinavir with HIV-1 protease in comparison between the wild-type and G48V and G48V/L90M mutants based on QM and QM/MM calculations, J. Mol. Graph. Model. 26 (2007) 720–727.
[26] Y.-D. Chen, Y.-J. Jiang, J.-W. Zou, Q.-S. Yu, Q.-D. You, Identification of ligand features essential for HDACs inhibitors by pharmacophore modeling, J. Mol. Graph. Model. 26 (2008) 1160–1168.
[27] K. Bharatham, N. Bharatham, K.H. Park, K.W. Lee, Binding mode analyses and pharmacophore model development for sulfonamide chalcone derivatives, a new class of alpha-glucosidases inhibitors, J. Mol. Graph. Model. 26 (2008) 1202–1212.
[28] Y. Kurogi, O.F. Guner, Pharmacophore modeling and three-dimensional databases searching for drug design using catalyst, Curr. Med. Chem. 8 (2001) 1035–1055.
[29] C. Michaux, X. de Leval, F. Julemont, J.M. Dogne, B. Pirotte, F. Durant, Structure-based pharmacophore of COX2 selective inhibitors and identification of original lead compounds from 3D database searching method, Eur. J. Med. Chem. 41 (2006) 1446–1455.
[30] Accelrys, Inc. Discovery Studio 2.1, 10188 Telesis Court, Suite 100 San Diego, CA 92121-4779. U.S.A., 2008.
[31] J. Wang, R.M. Wolf, J.W. Caldwell, P.A. Kollman, D.A. Case, Development and testing of a general amber force field, J. Comput. Chem. 25 (2004) 1157–1174.
[32] S. Sekharan, A. Altun, K. Morokuma, QM/MM study of dehydro and dihydro β-lonone retinal analogues in squid and bovine rhodopsins: implications for vision in salamander rhodopsin, J. Am. Chem. Soc. 132 (2010) 15856–15859.
[33] S. Sekharan, A. Altun, K. Morokuma, Photochemistry of visual pigment in a Gq protein-coupled receptor (GPCR)-insights from structural and spectral tuning studies on squid rhodopsin, Chem. Eur. J. 16 (2010) 1744–1749.
[34] S. Sekharan, K. Morokuma, Drawing the retinal out of its comfort Zone: an ONIOM(QM/MM) study of mutant squid rhodopsin, J. Phys. Chem. Lett. 1 (2010) 668–672.
[35] A. Altun, S. Yokoyama, K. Morokuma, Spectral tuning in visual pigments: an ONIOM(QM:MM) study on bovine rhodopsin and its mutants, J. Phys. Chem. B 112 (2008) 6814–6827.
[36] S.F. Boys, F. Bernardi, The calculation of small molecular interactions by the differences of separate total energies, some procedures with reduced errors, Mol. Phys. 19 (1970) 553–566.
[37] M.J. Frisch, G.W. Trucks, H.B. Schlegel, G.E. Scuseria, M.A. Robb, J.R. Cheeseman, J.A. Montgomery Jr., T. Vreven, K.N. Kudin, J.C. Burant, J.M. Millam, S.S. Iyengar, J. Tomasi, V. Barone, B. Mennucci, M. Cossi, G. Scalmani, N. Rega, G.A. Petersson, H. Nakatsuji, M. Hada, M. Ehara, K. Toyota, R. Fukuda, J. Hasegawa, M. Ishida, T. Nakajima, Y. Honda, O. Kitao, H. Nakai, M. Klene, X. Li, J.E. Knox, H.P. Hratchian, J.B. Cross, C. Adamo, J. Jaramillo, R. Gomperts, R.E. Stratmann, O. Yazyev, A.J. Austin, R. Cammi, C. Pomelli, J.W. Ochterski, P.Y. Ayala, K. Morokuma, G.A. Voth, P. Salvador, J.J. Dannenberg, V.G. Zakrzewski, S. Dapprich, A.D. Daniels, M.C. Strain, O. Farkas, D.K. Malick, A.D. Rabuck, K. Raghavachari, J.B. Foresman, J.V. Ortiz, Q. Cui, A.G. Baboul, S. Clifford, J. Cioslowski, B.B. Stefanov, G. Liu, A. Liashenko, P. Piskorz, I. Komaromi, R.L. Martin, D.J. Fox, T. Keith, M.A. Al-Laham, C.-Y. Peng, A. Nanayakkara, M. Challacombe, P.M.W. Gill, B. Johnson, W. Chen, M.-W. Wong, C. Gonzalez, J.A. Pople, Gaussian 03, Gaussian, Inc., Wallingford, CT, 2003.
[38] M. Chopra, R. Gupta, S. Gupta, D.J. Saluja, Molecular modeling study on chemically diverse series of cyclooxygenase-2 selective inhibitors: generation of predictive pharmacophore model using Catalyst, J. Mol. Model. 14 (2008) 1087–1099.
[39] G.M. Morris, R. Huey, W. Lindstrom, M.F. Sanner, R.K. Belew, D.S. Goodsell, A.J. Olson, Autodock4 and AutoDockTools4: automated docking with selective receptor flexibility, J. Comput. Chem. 30 (2009) 2785–2791.
[40] D.F. Corbett, K.A. Dwornik, D.M. Garrido, S.C. Mckeown, W.Y. Mills, A.J. Peat, T.L. Smalley Jr., GlaxoSmithKline plc. (2005), WO2005051890.
[41] T. Yasuma, S. Kitamura, N. Negoro, Takeda Pharmaceuticals (2005), WO2005063729.
[42] T. Yasuma, S. Kitamura, N. Negoro, Takeda Pharmaceuticals (2005), WO2005095338.
[43] S.M.M. Sony, M.N. Ponnuswamy, Nature of pi-interaction in nitrogen-containing heterocyclic systems: a structural database analysis, Cryst. Crowth Des. 6 (2006) 736–742.
[44] S.-O. Suwipa, M. Kuno, S. Hannongbua, Binding energy analysis for wild-type and Y181C mutant HIV-1 RT/8-Cl TIBO complex structure: quantum chemical calculations based on the ONIOM method, Proteins 61 (2005) 859–869.
[45] S. Kristyán, P. Pulay, Can (semi) local density-functional theory account for the London dispersion forces, Chem. Phys. Lett. 229 (1994) 175–180.
[46] S.-Y. Lu, Y.-J. Jiang, J. Lv, T.-X. Wu, Q.-S. Yu, W.-L. Zhu, Molecular docking and molecular dynamics simulation studies of GPR40 receptor–agonist interactions, J. Mol. Graph. Model. 28 (2010) 766–774.
[47] S.B. Bharate, K.V.S. Nemmani, R.A. Vishwakarma, Progress in the discovery and development of small-molecule modulators of G-protein-coupled receptor 40 (GPR40/FFA1/FFAR1): an emerging target for type 2 diabetes, Expert Opin. Ther. Patents 19 (2009) 237–264.